

JOURNAL
— OF —
THE ROYAL
SOCIETY

ISSN 1742-5689

volume 6

number 41

pages 1103–1245

Interface



Cross-disciplinary Sciences



Royal Society **Publishing**

*Informing the science
of the future*

6 December 2009

Spine-shaped gold protrusions improve the adherence and electrical coupling of neurons with the surface of micro-electronic devices

Aviad Hai¹, Ada Dormann¹, Joseph Shappir²,
Shlomo Yitzchaik³, Carmen Bartic⁴, Gustaaf Borghs⁴,
J. P. M. Langedijk⁵ and Micha E. Spira^{1,*}

¹*Department of Neurobiology, The Life Sciences Institute,*

²*School of Engineering, and* ³*Institute of Chemistry, The Hebrew University of Jerusalem, Jerusalem, Israel*

⁴*IMEC vzw, MCP/ART, Leuven, Belgium*

⁵*Pepscan NV, Lelystad, The Netherlands*

Interfacing neurons with micro- and nano-electronic devices has been a subject of intense study over the last decade. One of the major problems in assembling efficient neuro-electronic hybrid systems is the weak electrical coupling between the components. This is mainly attributed to the fundamental property of living cells to form and maintain an extracellular cleft between the plasma membrane and any substrate to which they adhere. This cleft shunts the current generated by propagating action potentials and thus reduces the signal-to-noise ratio. Reducing the cleft thickness, and thereby increasing the seal resistance formed between the neurons and the sensing surface, is thus a challenge and could improve the electrical coupling coefficient. Using electron microscopic analysis and field potential recordings, we examined here the use of gold micro-structures that mimic dendritic spines in their shape and dimensions to improve the adhesion and electrical coupling between neurons and micro-electronic devices. We found that neurons cultured on a gold-spine matrix, functionalized by a cysteine-terminated peptide with a number of RGD repeats, readily engulf the spines, forming tight apposition. The recorded field potentials of cultured *Aplysia* neurons are significantly larger using gold-spine electrodes in comparison with flat electrodes.

Keywords: cell adhesion; phagocytosis; bio-electronic interface; seal resistance; field potential

1. INTRODUCTION

Interfacing cultured cells with the substrates on which they grow has been a subject of intense study as the nature of this contact influences the morphology, growth patterns and physiology of the cells (see the review by Spatz & Geiger 2007). Successful employment of micro-electronic technologies to produce devices for recording and stimulation of excitable cells also depends on the nature of the interface formed between neurons and the surface of the electronic device (Fromherz 2003; Braun & Fromherz 2004; Gleixner & Fromherz 2006; Wrobel *et al.* 2008). In fact, the level of electrical coupling between neurons and the electrical components is limited by the dimensions of the cleft formed between the cells and the surface of the sensing pads (Fromherz 2003).

Experimental results and theoretical considerations revealed that the signal-to-noise ratio of neuro-electronic

hybrids is determined by three main factors: (i) the recording device noise level, (ii) the seal resistance formed between the neuron and the sensing element of the electronic device (R_{seal}), and (iii) the intensity of the current generated by the neuron's activity (Cohen *et al.* 2006, 2008). Although the intensity of the currents generated by propagating action potentials can be experimentally modulated by pharmacological manipulations or over-expression of ion channels, such manipulations would change the electro-anatomy and excitable 'fingerprints' of the cells and thus alter the network properties. For that reason, a large number of studies attempt to improve R_{seal} . Since R_{seal} is defined by the width of the extracellular cleft formed between the cell and the substrate (d_j), the resistivity of the material within the cleft (ρ_j) and its planar dimensions (a_j), efforts are devoted to reduce d_j and increase the contact area. The main approaches reported in the literature are (i) to chemically functionalize the substrate on which the neurons grow with proteins that promote stronger adhesion

*Author for correspondence (spira@cc.huji.ac.il).

and reduce d_j (e.g. Lim & Donahue 2007; Cai *et al.* 2008; Wrobel *et al.* 2008); (ii) to alter the surface topography on which the neurons grow (see the reviews by Sniadecki *et al.* 2006; Spatz & Geiger 2007); and (iii) by applying mechanical pressure to compress restricted neuronal compartments against the sensing pads (Jenkner & Fromherz 1997; Cohen *et al.* 2008). Aside from the third approach, which resulted in a significant increase in the amplitude of the recorded field potentials reaching semi-intracellular field potentials with amplitudes as high as 10–30 mV (Jenkner & Fromherz 1997; Cohen *et al.* 2008), the other approaches have not been shown to improve the electrical coupling in any significant manner.

Various methods that have been used to estimate the thickness of the cleft width formed between different cell types and substrates revealed that the cleft thickness ranges between 0 and 150 nm, averaging at 30–40 nm. For example, fluorescence interference-contrast microscopy of neurons and fibroblasts grown on laminin or fibronectin demonstrated cleft widths in the range of 40–100 nm (Lambacher & Fromherz 1996; Braun & Fromherz 1997; Iwanaga *et al.* 2001; Gleixner & Fromherz 2006). A cleft thickness of 45–65 nm was formed by HEK293 cells grown on oxide surfaces coated by collagen (Straub *et al.* 2001) or 70 ± 10 nm for HEK293 cells grown on fibronectin-coated substrates (Brittinger & Fromherz 2005). A recent systematic study of the cleft width formed by HEK293 cells using thin sections prepared for transmission electron microscopy (TEM) by Wrobel *et al.* (2008) revealed that the cleft width formed between cells and a smooth silicon oxide substrate is not homogeneous, varying from tight attachment of 0–10 nm in 5–20% of the contact area to low adhesion of 100–150 nm in the remaining areas. The average cleft thickness in this study was estimated to be 35–40 nm. It is interesting to note that conventional substrates used for cell cultures, such as poly-L-lysine (PLL), poly-D-lysine, extracellular matrix (ECM) gel and fibronectin, lead to closer adhesion of cells than that of laminin and concanavalin A. Nevertheless, the frequency of tight contacts, in the range of 0–10 nm, was found to be independent of the type of protein coating. In conclusion, examination of the literature suggests that the use of conventional substrate materials for culturing of cells does not improve the cell–substrate physical contact and therefore is not expected to significantly improve the levels of electrical coupling between excitable cells and sensing pads.

In the present study, we experimentally evaluated the use of micro-structures that protrude from the substrate to enhance adhesion and improve the electrical coupling. Our approach is based on the naturally occurring phenomenon of particle phagocytosis by living cells. Phagocytosis is defined as the cellular process that leads to the internalization of large particles of up to 0.5 μm into the cells (see the reviews by Stuart & Ezekowitz 2005; Huynh *et al.* 2007). It is a process in which extensions of the plasma membrane are formed around a particle, where the particle ‘sinks’ into the cell leading to its internalization (figure 1*a*). The main steps leading to the

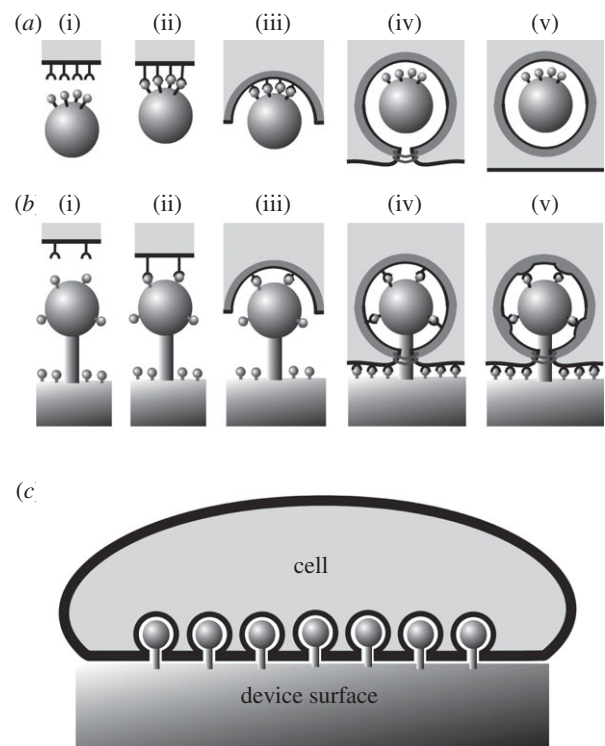


Figure 1. The engulfment of gold spines by a cell is based on mimicry of phagocytosis. (a) Phagocytosis of particles by cells is generated by binding of receptor molecules presented on the surface of the cell to molecules presented by the target particle (the immobilized ligand is shown at the tip of the particle; however, it should be noted that it is homogeneously applied to the entire surface of the particle and the spine). The interaction tethers the target to the membrane (i, ii). Additional receptors are recruited to the target leading to increased contact between the target and the plasma membrane and initiating the extension of the plasma membrane around the particle (ii). Signalling from the cytoplasmic domain of the engaged receptors recruits a family of proteins around the particle (iii—the assembly of the various proteins is depicted by the dark grey layer). Actin filaments together with myosin and other proteins generate the mechanical force to drive the process of particle engulfment into the cell (iv). The plasma membrane surrounding the particle is pinched off from the plasma membrane (v). The detached vacuole that contains the particle is now free to move in the cytosol and fuse with endosomes. (b) The internalization of a gold spine requires the cell to ‘swallow’ its head, but not to ‘finish off’ the process of vacuole formation. (c) Gold spines on the active surface of a semiconductor device.

internalization of a particle by phagocytosis are: (i) the interaction between the extracellular domains of receptor molecules presented by the cell and molecules presented on the target surface that tethers the target to the membrane (figure 1*a*(i)(ii)); (ii) signalling by the cytoplasmic domain of the engaged receptors recruits a number of proteins that construct the molecular machinery to internalize the particle (figure 1*a*(iii)), the assembly of the various proteins is depicted by the dark grey layer; and (iii) the plasma membrane surrounding the particle is pinched off from the plasma membrane (figure 1*a*(iv)(v)). The detached plasma membrane that contains the particle is now free to move in the cytosol and fuse with endosomes.

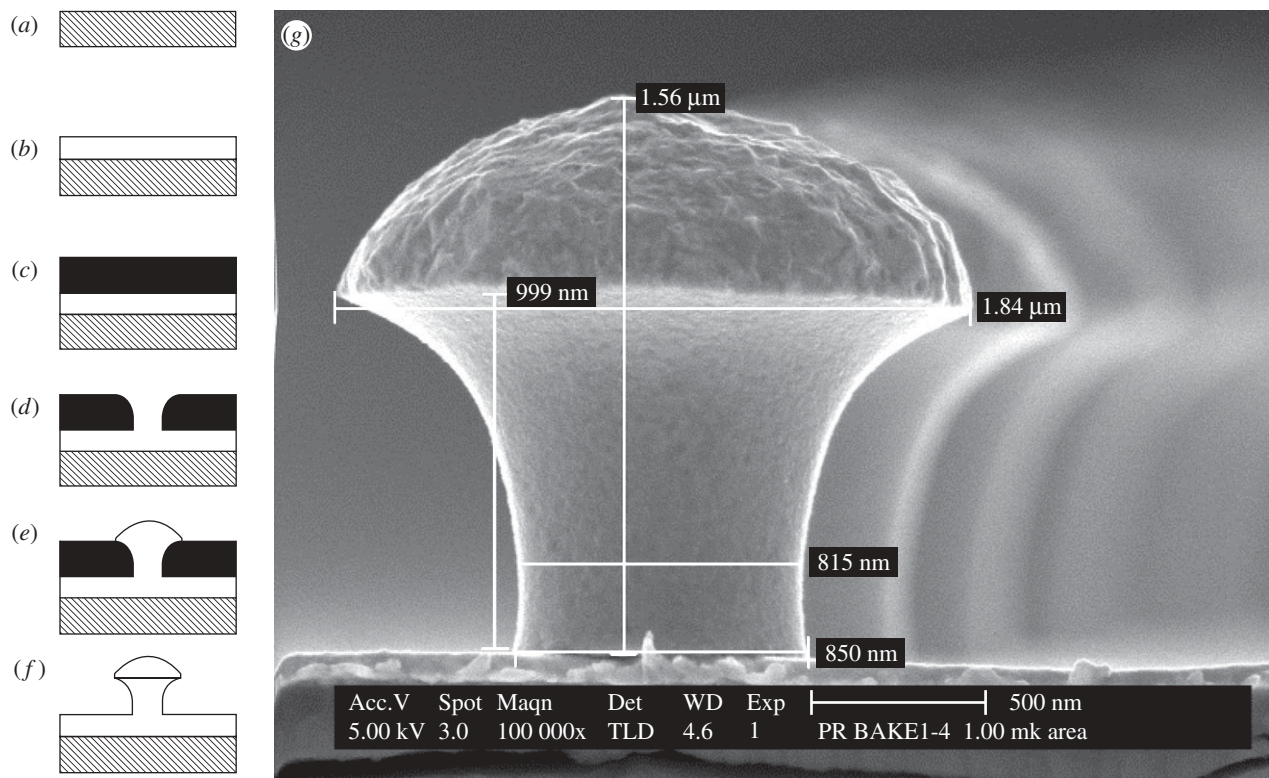


Figure 2. Fabrication of gold spines. Silicon or glass samples (a) are coated with a Cr/Au layer (b) using sputtering techniques and are then spin coated with photoresist material (c). Samples undergo photolithography using a photomask to open holes through the photoresist (d). The artificial gold spines are then formed on the surface by way of gold electroplating (e) and finally the photoresist layer is removed (f). (g) Scanning electron microscopic image of gold spines fabricated on a glass surface.

Using electron microscopic analysis and measurements of field potentials generated by action potentials, we examined here the use of micro-structures that imitate dendritic spines in their shape and dimensions. Dendritic spines are small protrusions in the range of a few micrometres scattered along dendrites of the majority of neurons in the nervous system (Matus 2005) where they serve as the post-synaptic sites. The geometry of the spines plays prominent roles in signal transmission at excitatory synapses (Roelandse *et al.* 2003). We hypothesized that similar to the phagocytosed particle (figure 1a), the gold spine will be engulfed by the plasma membrane (figure 1b). Nevertheless, unlike the particle, the gold-spine-like protrusions will be 'swollen' by the cell, but the process of internalization will end at a stage in which the plasma membrane tightly surrounds the head and stalk of the gold spine (figure 1b(v)).

We found that cells cultured on a gold-spine matrix readily engulf the spines forming tight membrane apposition. The field potentials generated by action potentials of cultured *Aplysia* neurons are significantly larger when neurons are cultured on gold spines in comparison with the field potentials recorded by flat electrodes.

2. METHODS

2.1. Fabrication of gold-spine-like matrix for structural studies and electrical recordings

The structural studies were performed on gold-spine-like matrices fabricated on a conventional microscope cover

glass (Marienfeld, Germany). The cover glass surface was coated with a Cr (20 nm)/Au (200 nm) blanket seed layer by sputtering. Samples were then dehydrated for 30 min (120°C), spin-coated with photoresist S-1813 (4000 r.p.m.) and baked for 30 min (90°C) after which they were exposed to UV using a photomask with approximately 0.75–1.25 μm holes determining the stem diameter of the spine (Karl Susse MJB UV400 mask aligner, $W = 44 \text{ mW cm}^{-2}$, exposure time: 4.4–4.6 s). Development was done using MF-319 for 20 s after which the developing agent was washed from the samples twice in de-ionized water. Gold spines were then electrodeposited (Neutronex 309 plating solution) at a current density of 0.15 A dm^{-2} for 15 min. The photoresist layer was then stripped using acetone. Glass slides were attached to culture dishes using Sylgard (Dow Corning) and were then dried (48 h, 60°C).

Gold spines for electrical measurements were prepared on silicon wafers as described by Huys *et al.* (2008). Briefly, the electrodes were patterned by the Cu-damascene method. A diffusion barrier made of 50 nm SiC and 50 nm Si₃N₄ was deposited on top of the metal in order to prevent diffusion of Cu through the upper layers. A 1.4 μm layer of SiO₂ was then deposited by PECVD at 400°C on top. Holes with diameters ranging from 250 nm to 1 μm were formed at the tip of the electrode lines by deep-reactive ion etching selective to the Cu metal (all fabrications up to this stage were conducted at IMEC, Belgium). Gold spines were then electrodeposited through the holes (Neutronex 309 plating solution) at a current density of 0.15 A dm^{-2} for 15 min, similar to the procedures used for the glass slides described earlier. The device was

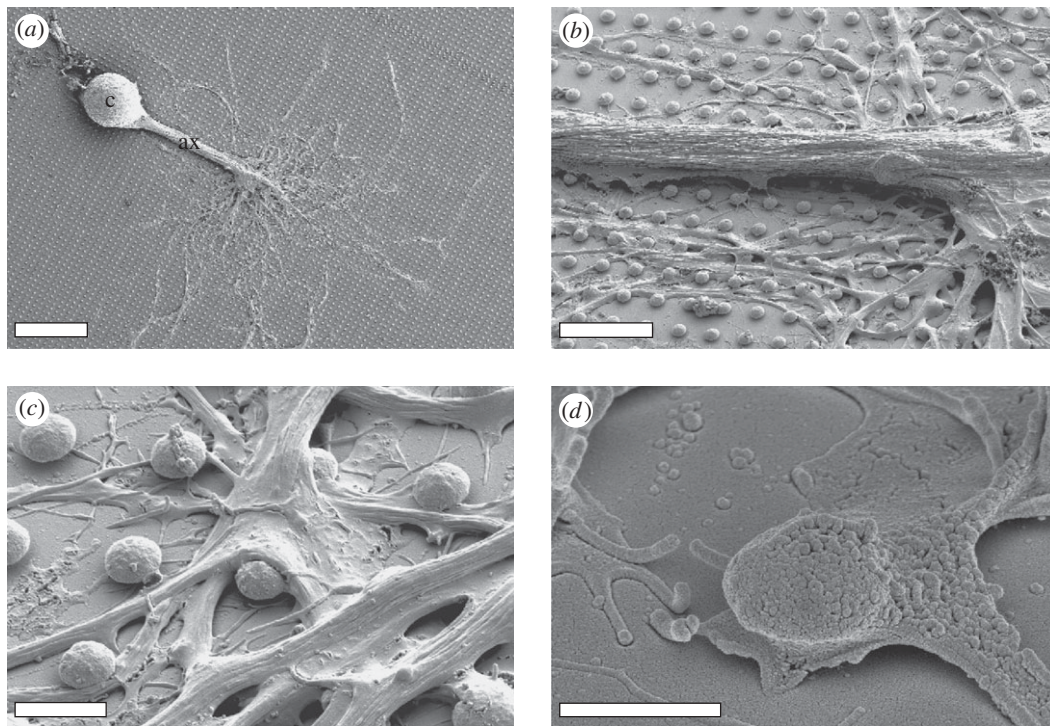


Figure 3. Scanning electron microscopic images of neurons isolated from *Aplysia* grown on gold-spine matrices. (a) A low magnification image of an entire neuron (c, cell body; ax, the main axon from which neurites extend in various directions). (b) Enlargement of the main and branching neurites. (c) Close-up of the neurites and gold-spine heads. (d) A single neurite engulfing a gold spine. Scale bars, 100, 20, 5 and 2 μm for (a), (b), (c) and (d), respectively.

designed such that the conductive lines terminated with a single or four gold spines (the reported field potential recordings were made using the four-spine electrodes). Wafers were then sawn and underwent manual bonding to 28-pin dual-inline packages. The resulting devices were attached to culture dishes using epoxy (EPO-TEK 375, Epoxy Technology, 120°C, 40 min).

2.2. Surface functionalization

To improve the adhesion of the neurons to the gold substrate, we used a cysteine (C)-terminated peptide with a number of RGD repeats (R = arginine, G = glycine, D = aspartic acid and a long decalysine (K)₁₀ spacer) to imitate ECM proteins (Toublan *et al.* 2006). We refer to this peptide as engulfment promoting peptide (EPP)—CKKKKKKKKKKK-PRGDMPRGDMPRGDMPRGDM (MW 3630 g mol⁻¹). The peptide was initially prepared at Pepsan NV, The Netherlands and then by Biosight, Israel. The Au substrates were immersed in EtOH for 20 min in order to remove any pre-formed oxide layers. Functionalization of the gold surface was done by application of 1 mM EPP, in phosphate-buffered solution (PBS), at room temperature, for 16 h. The functionalized substrates were washed excessively with PBS.

2.3. Cell culture

Left upper quadrant (LUQ) neurons from the abdominal ganglia of *Aplysia californica* were isolated and maintained in culture as described previously (Schacher & Proshansky 1983; Spira *et al.* 1996). Briefly, juvenile *Aplysia* (1–10 g) supplied from the University of

Miami, National Resource for *Aplysia*, were anaesthetized by injecting isotonic MgCl₂ solution (380 mM) into the animal's body cavity. Buccal and abdominal ganglia were dissected and incubated in L-15 supplemented for marine species (ms L-15) containing 1 per cent protease (type IX, Sigma-Aldrich, Rehovot, Israel) at 34°C for 1.5–2.5 h. Following the protease treatment, the ganglia were desheathed. Individual neurons were manually pulled out along with their original axon with the aid of a sharp glass micro-electrode and plated on the devices.

Cell lines including mouse embryonic fibroblast cells (NIH/3T3), Chinese hamster ovary cells (CHO), rat adrenal medulla cells (PC-12) and rat myocardium cells (H9C2) were propagated in Dulbecco's modified Eagle's medium containing 10 per cent foetal calf serum, L-glutamine and antibiotics (materials purchased from Biological Industries, Israel) and plated on EPP-coated devices. All cell types were cultured for 48 h before fixation for TEM. For the electrophysiological experiments, *Aplysia* neurons were cultured on the gold-spine device for 48 h.

2.4. Electron microscopy

Cells cultured on the gold-spine substrate were fixed and then dehydrated and embedded in Agar 100 within the culturing dish as described previously (Spira *et al.* 2003). Briefly, *Aplysia* neurons and the other cell types were fixed by 3 per cent glutaraldehyde in artificial sea water (ASW) or phosphate buffer at pH 6.9 (respectively). The cells were then washed in ASW or phosphate buffer and then in 0.5 M cacodylate

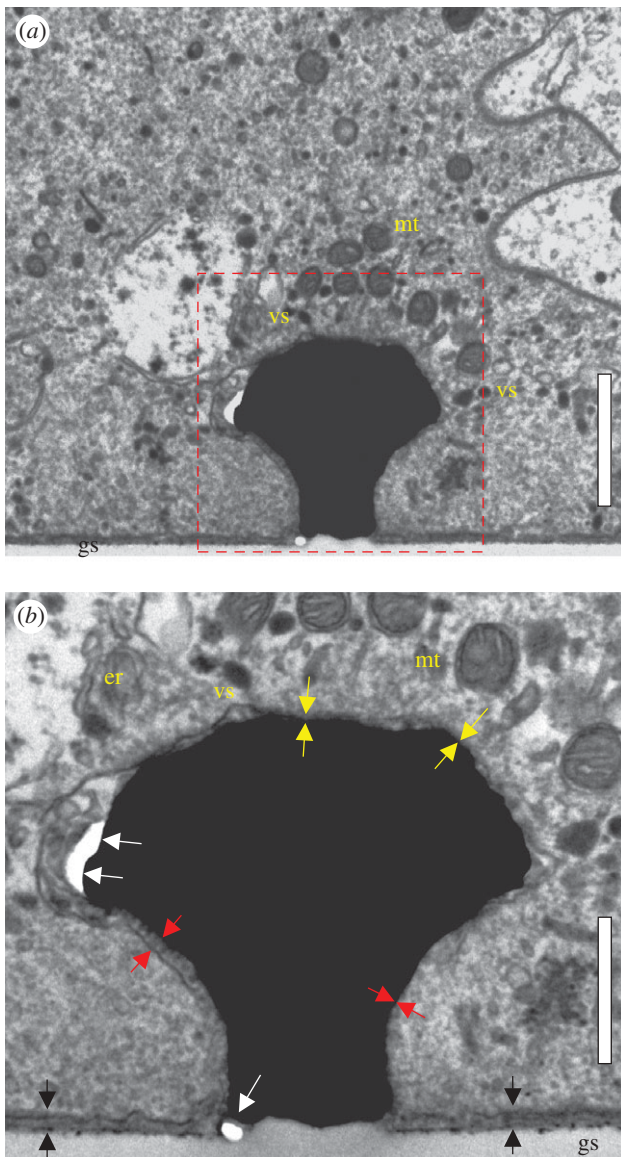


Figure 4. Transmission electron microscopic images of a gold spine engulfed by an *Aplysia* neuron. (a) Low magnification image of a neuron engulfing a gold spine coated with EPP. The quality of the fixation is evident by the preservation of the organelles (mt, mitochondria; vs, vesicle; er, endoplasmic reticulum; gs, area of flat gold substrate; scale bar, 1 μm). (b) Enlargement of the red box shown in (a). The gap formed between the plasma membrane and the flat surface is 30–50 nm (black arrows). The gap between the spine structure and the plasma membrane is approximately 30 nm, but in some areas it cannot be defined and seems to be zero (yellow arrows, spine head; red arrows, spine stalk). White arrows indicate regions where the embedding polymer was torn most probably by post-embedding mechanical tension (for details, see text; scale bar, 500 nm).

buffer, pH 7.4 (Agar Scientific, Stansted, UK). All cell types were post-fixed in 0.5 per cent osmium tetroxide (Next Chimica, Centurion, South Africa) and 0.8 per cent $\text{K}_3\text{Fe}(\text{CN})_6$. Dehydration was carried out through a series of ethanol solutions, and finally the neurons were embedded in Agar 100 (Agar Scientific). Then the glass substrate was etched using 30 per cent hydrofluoric acid (for approx. 3 h). The Cr/Au layer was

partially etched by diluted Au etcher ($\text{I}_2/\text{KI}/\text{H}_2\text{O}$) and diluted HF (1 : 40), leaving the gold-spine structures intact. Thereafter, the agar block, including the cells, was re-embedded in Agar 100 in a flat mould. This doubly embedded preparation was then thin-sectioned.

Measurements of cleft width from TEM images were done digitally using image analysis program ImageJ. For each cell type, four or five cells were chosen, and one engulfed gold spine was analysed. Altogether 23 junctions formed between the cells and the gold-spine substrate was analysed. Each TEM image of an engulfed spine was divided into three areas: (i) gold-spine head; (ii) gold-spine stalk; and (iii) the flat gold substrate between the gold spines. The cleft width was measured along 30 points at evenly spaced intervals along the cleft at each of the three areas mentioned earlier. Significance of the difference between average cleft width values of the different areas was analysed using one-way ANOVA.

2.5. Electrophysiology

Conventional intracellular recording and stimulation of cultured *Aplysia* neurons were used as described previously by our laboratory (Cohen *et al.* 2004, 2006, 2008). The micro-electrodes were pulled from 1.5/–1.02 mm borosilicate glass tubes with filaments and filled with 2 M KCl. Electrode resistance ranged between 4 and 10 $\text{M}\Omega$. For intracellular recording and stimulation, the micro-electrode tip was inserted into the cell body.

2.6. Device recording

For the recording with standard flat electrodes, we used Multichannel Systems (Reutlingen, Germany) electrode arrays (60 Ti/Au/TiN electrodes, 10 μm diameter, 200 μm spacing). For the experiments, silicone nitride insulating layer was coated with either PLL or EPP. Both commercial devices and artificial spine electrode devices were amplified by a 60-channel amplifier (B-MEA-1060, Multichannel Systems), with frequency limits of 1–5000 Hz and a gain of 1200. Spine electrode devices were mounted on a custom printed circuit adapter (Olimex, Bulgaria) attached to the commercial amplifier (generating higher noise level).

2.7. Computer simulation

Simulations of action potentials generated by a neuron composed of a cell soma, axon hillock and an axon were conducted using the 'NEURON' multi-compartmental simulation model (Hines and Carnevale 1997) and as previously described by our laboratory (Cohen *et al.* 2006). Simulation of field potentials recorded by flat electrodes and 'gold-spine' electrodes was conducted using the built-in extracellular simulation. We constructed a neuron composed of a cell body with a diameter of 100 μm and a cylindrical axon with a diameter of 10 μm . As in our earlier study, we used the Hodgkin & Huxley (H&H) model parameters to simulate the generation of action potentials (Hodgkin & Huxley 1952) rather than to embed the specific parameters of *Aplysia* neurons. The simulated

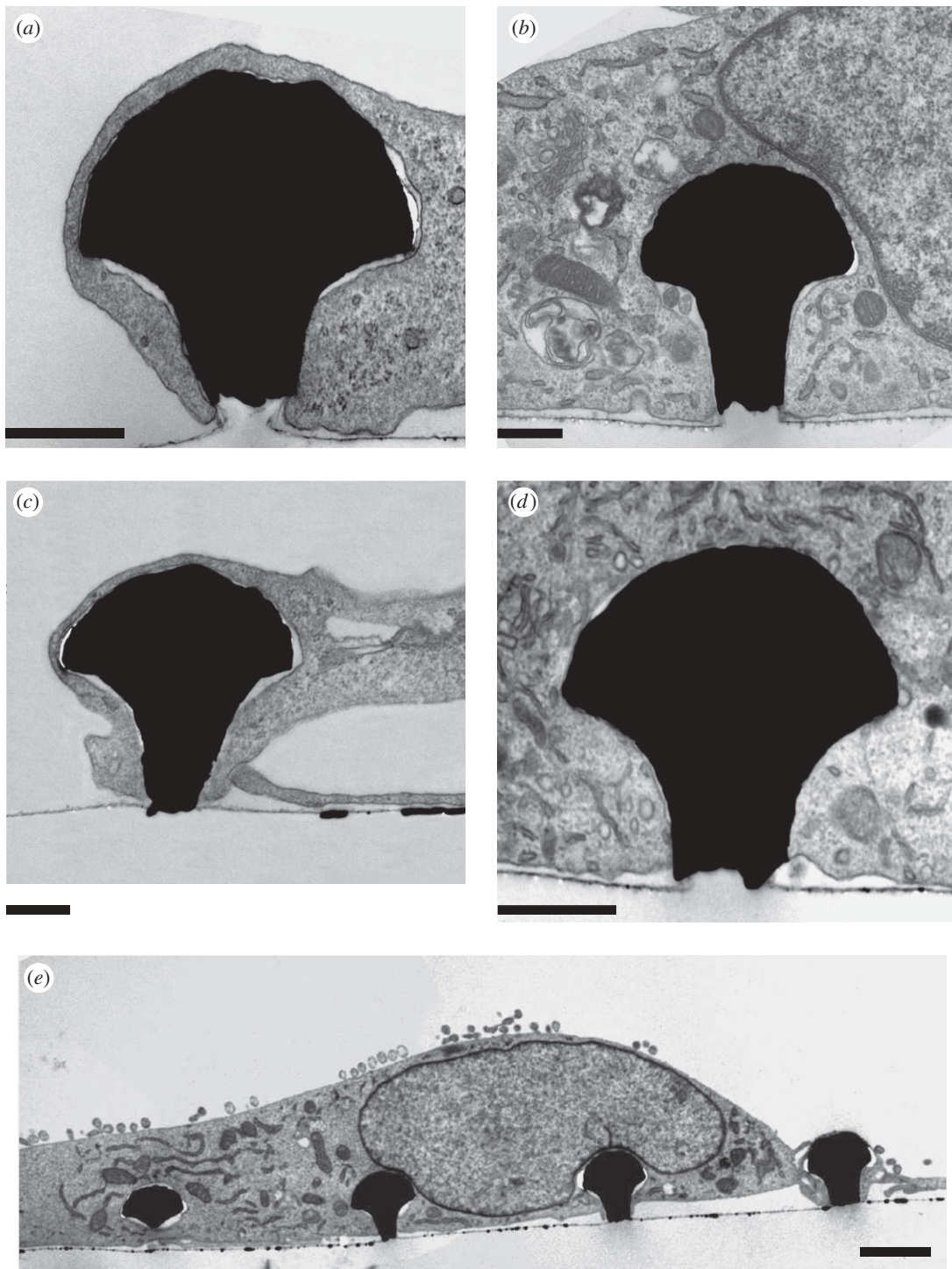


Figure 5. Transmission electron microscopic images of gold spines engulfed by various cell types: (a) CHO, (b) fibroblasts (3T3), (c) cardiomyocytes (H9C2) and (d) rat adrenal medulla cells (PC-12). (e) Engulfment of multiple gold spines by 3T3 cells. Scale bars, 500 nm (a, b, c and d) and 2 μm (e).

neurons had a resting potential of -65 mV, access resistance of 3.2 M Ω , maximum sodium conductance of 0.120 S cm^{-2} in the soma and axon and 0.138 S cm^{-2} in the more excitable axon hillock (Cohen *et al.* 2006), maximum potassium conductance of 0.026 S cm^{-2} , leak conductance of 0.003 S cm^{-2} and leak current reversal potential of -54.3 mV. The cell soma was divided into sections according to the ratio between the dimensions of the flat or spine electrode and the cell soma. The

extracellular structure contained one extracellular layer and had the following parameters: (i) axial resistance (xradial) of $2.12\text{--}67$ M Ω cm^{-1} in accordance with the cleft width measured visually from TEM images; (ii) lateral conductance of 0.2 mho cm^{-2} ; and (iii) lateral capacitance of 30 μF cm^{-2} for the gold spine electrodes and 0.064 μF cm^{-2} for the flat electrodes. All other parameters were taken from the H&H model (Hodgkin & Huxley 1952).

Table 1. Average width values (nm) of the cleft formed between the plasma membrane of various cell types and the flat gold surface in between the spines, spine stalk and a spine head, according to the analysis of TEM images. The fifth column depicts the significance of the difference between average cleft width values of the different areas examined (analysed using one-way ANOVA). Number of points measured $n = 150$ in the case of 3T3, H9C2 and PC-12 cells and $n = 120$ for *Aplysia* and CHO cells.

cell type	flat surface (nm)	spine stalk (nm)	spine head (nm)	F-value
<i>Aplysia</i>	56 ± 29	35 ± 21	30 ± 17	$F_{2,357} = 43.5, p < 0.001$
CHO	89 ± 66	31 ± 28	21 ± 16	$F_{2,357} = 89.6, p < 0.001$
3T3	80 ± 63	38 ± 35	16 ± 10	$F_{2,447} = 90.7, p < 0.001$
H9C2	123 ± 75	49 ± 41	50 ± 32	$F_{2,447} = 97.6, p < 0.001$
PC-12	145 ± 118	31 ± 28	27 ± 24	$F_{2,447} = 132.4, p < 0.001$

3. RESULTS

3.1. Fabrication of artificial gold spines

Artificial gold spines were fabricated on glass and silicon substrates (figure 2). The glass and silicon samples were first coated with a Cr/Au layer (figure 2*b*) by sputtering and then spin coated with the photoresist material (figure 2*c*). Photolithography was done on the resulting surface to open 1 μm diameter holes in the photoresist layer (figure 2*d*). Gold spines were then grown through the holes by way of electrodeposition (figure 2*e*). Parameters and electroplating solution used generated a rough texture of the spine head (figure 2*g*), which increased its effective surface. Finally, the photoresist layer was stripped using acetone (revealing the spine structure, figure 2*f*). The dimensions and shape of the fabricated gold spines roughly imitate the shape of naturally occurring dendritic spines (Roelandse *et al.* 2003), with a stem height of approximately 1 μm , diameter of approximately 800 nm and a mushroom-shaped cap of 1.8–3 μm in diameter (figure 2*g*).

3.2. Engulfment of gold spines by cultured *Aplysia* neurons

Neurons were cultured on a matrix of gold spines fabricated on glass slides sputtered by a thin film of gold (§2), at an inter-spine interval of 8 μm and functionalized by EPP. Scanning electron microscopy of cultured *Aplysia* neurons on gold-spine matrix (figure 3) revealed a growth pattern that does not differ in any significant manner from that seen on a flat glass functionalized either by PLL or by EPP (Ziv & Spira 1998; Cohen *et al.* 2006). Scanning electron micrographs do not provide details on the intimate interface formed between the plasma membrane and the gold substrate. We therefore turned to examine thin sections for TEM.

Aplysia neurons (or other cell types, see below) grown on flat glass cover slides coated by PLL adhere to the substrate forming a cleft that ranges between 20 and 100 nm, while occasionally the cleft dimension can be larger than 100 nm (Oren *et al.* 2004). *Aplysia* neurons grown on gold-spine matrix coated with EPP as described earlier engulf the gold spines, forming intimate contact with the flat substrate (between the spine-like structures) and the heads and stalks of the spines (figure 4). Thin sections prepared for electron microscope observations often revealed that the cell body or main neurites tightly engulf a number of spines (figure 5*e*). The average width of the cleft formed between the

plasma membrane of cultured *Aplysia* neurons and the flat gold substrate between the spines is 56 ± 29 nm (table 1, figure 6*a*, black bars, 120 points along the clefts, $n_{\text{cells}} = 4$). Consistently, the neurons engulf the spines along the spine stalk and head, with an average cleft width of 35 ± 21 nm (table 1, figure 6*a*, red bars, 120 points along the cleft, $n_{\text{cells}} = 4$) and 30 ± 17 nm (table 1, figure 6*a*, blue bars, 120 points along the cleft, $n_{\text{cells}} = 4$), respectively. It should be noted that in many of the electron micrographs, the plasma membrane appears to be in direct contact with the spine head and stalk (i.e. without a discernable space between the plasma membrane and the gold spine; see figure 4*b*, yellow arrows), suggesting a significantly tighter cleft between the plasma membrane and the gold spine compared with the flat gold surface between the spines ($F_{2,357} = 43.5, p < 0.001$, one-way ANOVA). In fact, we estimate that 10 per cent of the contact area between the plasma membrane and the spine stalk and 12.5 per cent of the contact area with the spine head form close adhesion with the cleft width in the range of 0–10 nm (table 2). In contrast, the gap formed along the flat surface between the spines maintains a cleft of 56 ± 29 nm.

The difference in the cleft width formed at the neuron–spine interface and the neuron–flat substrate interface could result from mechanical stretching of the plasma membrane around the gold spine head by cytoskeletal elements that assemble around these structures, attributing the close adhesion to natural mechanical forces generated by the cell (McMahon & Gallop 2005; Gimsa *et al.* 2007). An alternative explanation would be that mechanical tension is generated during the processes of chemical fixation, dehydration, embedding and/or sectioning. It should be noted that the quality of the neuron fixation is good as evidenced by the very well-preserved structure of the mitochondria, vesicles, the endoplasmic reticulum and the plasma membrane facing the bathing medium (figure 3, §4).

3.3. Engulfment of gold spines by cultured vertebrate cells

To examine whether functionalized gold spines promote engulfment by cell types other than *Aplysia* neurons, we cultured a number of cell lines on the EPP-coated gold-spine matrix. We found that similar to *Aplysia* neurons, CHO (figure 5*a*), fibroblasts (3T3 cell line; figure 5*b*), cardiomyocytes (H9C2 cell line; figure 5*c*) and rat

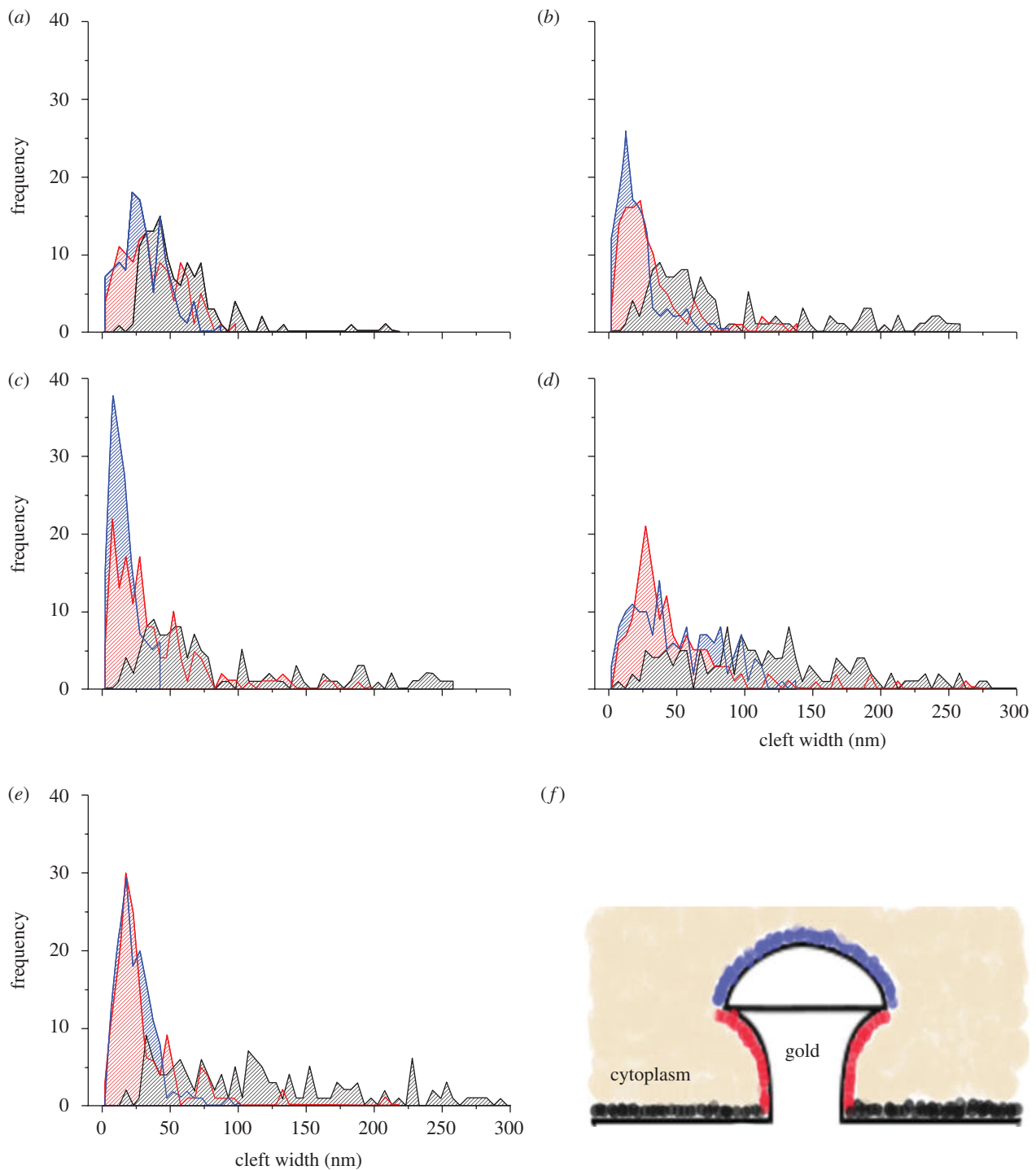


Figure 6. Analysis of the cleft formed between various cell types and the gold spines and surface. Cell types tested are (a) *Aplysia* neurons ($n_{\text{points}} = 150$; $n_{\text{cells}} = 5$), (b) CHO ($n_{\text{points}} = 120$; $n_{\text{cells}} = 4$), (c) fibroblast (3T3) cells ($n_{\text{points}} = 120$; $n_{\text{cells}} = 4$), (d) cardiomyocytes (H9C2) ($n_{\text{points}} = 150$; $n_{\text{cells}} = 5$) and (e) rat adrenal medulla cells (PC-12) ($n_{\text{points}} = 150$; $n_{\text{cells}} = 5$). (f) Cleft width was measured in three distinct areas: the flat substrate (black), spine stalk (red) and upper segment of the spine head (blue). Areas of rupture of agar, appearing as clear white areas in the electron microscopic images, were not included in the analysis (for details, see text).

adrenal medulla cells (PC-12 cell line; figure 5d) engulf a number of gold spines in a manner similar to that of cultured *Aplysia* neurons. Cleft width values of these cells are also similar to those generated by *Aplysia* neurons (figure 6 and tables 1 and 2), and significantly tighter adhesion to the spine is also observed compared with the adhesion to the flat gold surface near the spine

(table 1, column 5, F -values generated using one-way ANOVA).

3.4. Sensing action potentials by the gold spines

To examine whether the spine-like structures and the EPP improve the electrical coupling between the

Table 2. Percentage of the areas where the cleft width is in the range of 0–10 nm in various cell types.

cell type	flat surface (%)	spine stalk (%)	spine head (%)
<i>Aplysia</i>	0	10	12.5
CHO	0	14.2	24.2
3T3	0.7	18.7	35.3
H9C2	0.6	4	7.3
PC-12	0	10	10.7

neurons and the sensing device, we compared the field potentials generated by cultured *Aplysia* neurons grown on flat electrodes (Multichannel Systems) with those grown on gold-spine electrodes. For the experiments, *Aplysia* neurons were grown either on the flat multi-electrode array or on gold-spine multi-electrode arrays. Forty-eight hours after plating, a neuron cultured on the substrate was impaled with a sharp glass micro-pipette for both current injection and voltage recording. The field potentials generated by the evoked action potentials were recorded using an identical amplifier (figure 7*a,c*). The field potentials recorded by the commercially available flat electrodes ($n=6$) and the configuration of four gold-spine devices ($n=5$) demonstrated an average amplitude of 165 ± 104 and $770 \pm 294 \mu\text{V}$, respectively ($p < 0.05$, t -test). Recordings from a single gold spine generated field potentials similar to or even slightly smaller than the flat electrodes. The signal-to-noise ratio was 8.93 ± 4.74 for the gold-spine electrodes and 6.51 ± 4.35 for the flat electrodes ($p > 0.05$, t -test).

4. DISCUSSION

The main findings of the present study are that chemically functionalized gold-spine-like protrusions that extend from a flat surface are tightly engulfed by cultured neurons and thereby increase the neuron–substrate adherence and electrical coupling. Transmission electron microscopic analysis of the interfaces formed between cells and the gold-spine-like protrusions revealed that all cell types tested including *Aplysia* neurons, CHO, embryonic fibroblast cells (NIH/3T3), rat adrenal medulla cells (PC-12) and rat myocardium cells (H9C2) engulf the head and stalk of the gold spines. Examination of electron micrographs revealed that, on average, along approximately 15 per cent of the cell–gold spine interface, the extracellular cleft is in the range of 0–10 nm (table 2).

The assessment of the nature of the extracellular cleft formed between the plasma membrane of living cells and the gold substrate (as well as any other artificial substrate) by TEM must be done with great caution as the procedures of chemical fixation, dehydration, embedding and sectioning might generate alterations in the intracellular osmotic pressure and thereby generate structural artefacts (Studer *et al.* 2008).

Our morphometric analysis clearly revealed that the narrowest cleft was consistently formed between the cells and the gold-spine heads rather than with

the flat gold substrate between the gold spines (tables 1 and 2). It is conceivable to assume that the engulfment of the three-dimensional spine structure, by the aid of actin and other submembrane cytoskeletal elements and molecular motors, generates mechanical tension around the curving geometry of the spine. This mechanical tension and the submembrane proteins that generate it may underlie the formation of a narrow cleft between the plasma membrane and the spine's head and stalk. Nevertheless, there exists a possibility that the tight apposition formed between the plasma membrane and the spines may be a fixation artefact.

As is evident from the well-preserved shape, dimensions and integrity of the subcellular organelles in the electron micrographs, the fixation, dehydration and embedding procedures did not produce osmotic pressure artefacts (figures 3 and 4). The presence of electron translucent breaks within the embedding material, mainly (but not exclusively) at the curving junctions between the cells and the spine head as well as the stalk (e.g. figure 4*b*, white arrows), suggests that mechanical tension generated within the embedding polymer (Agar 100) leads to the detachment of the plasma membrane from the surface of the gold-spine head only during sectioning of the agar block or the observations rather than at earlier stages of the procedures.

It should be noted that the cleft formed between the flat gold substrate (between the gold spines) and the cell membrane maintains relatively large dimensions with an average cleft width of 56 ± 29 nm. Although the large error values may indicate variable cleft width, the cleft width along the flat gold substrate is rarely reduced to values < 10 nm (table 2). Since the chemical functionalization of the flat gold substrate between the spines and the gold spines themselves is identical, the differences in the average cleft width and, in particular, the percentage of surface area revealing tight adhesion (< 10 nm) could be related to the different geometries of the curving spines compared with the flat substrate between them. Whereas active engulfment of the three-dimensional spine structure and the recruitment of adhesion molecules could underlie the generation of the narrow cleft, we emphasize that we cannot reject with certainty that the narrow clefts are artefacts generated by the procedures of chemical fixation, dehydration and embedding of the material. This aspect should be examined in the future in live preparations. Furthermore, the use of electron cryomicroscopy for the visualization of structures at the nanometre scale may also be used in the future to elicit the nature of the interface presented here at a higher resolution (see the review by Wang & Sigworth 2006).

4.1. Estimate of the seal resistance formed by the interaction between the plasma membrane and an engulfed gold spine from electron micrographs

The TEM images presented in the study revealed that the cleft between the neuron membrane and the gold spine is in the range of 0–40 nm (whereas 0–1 nm is

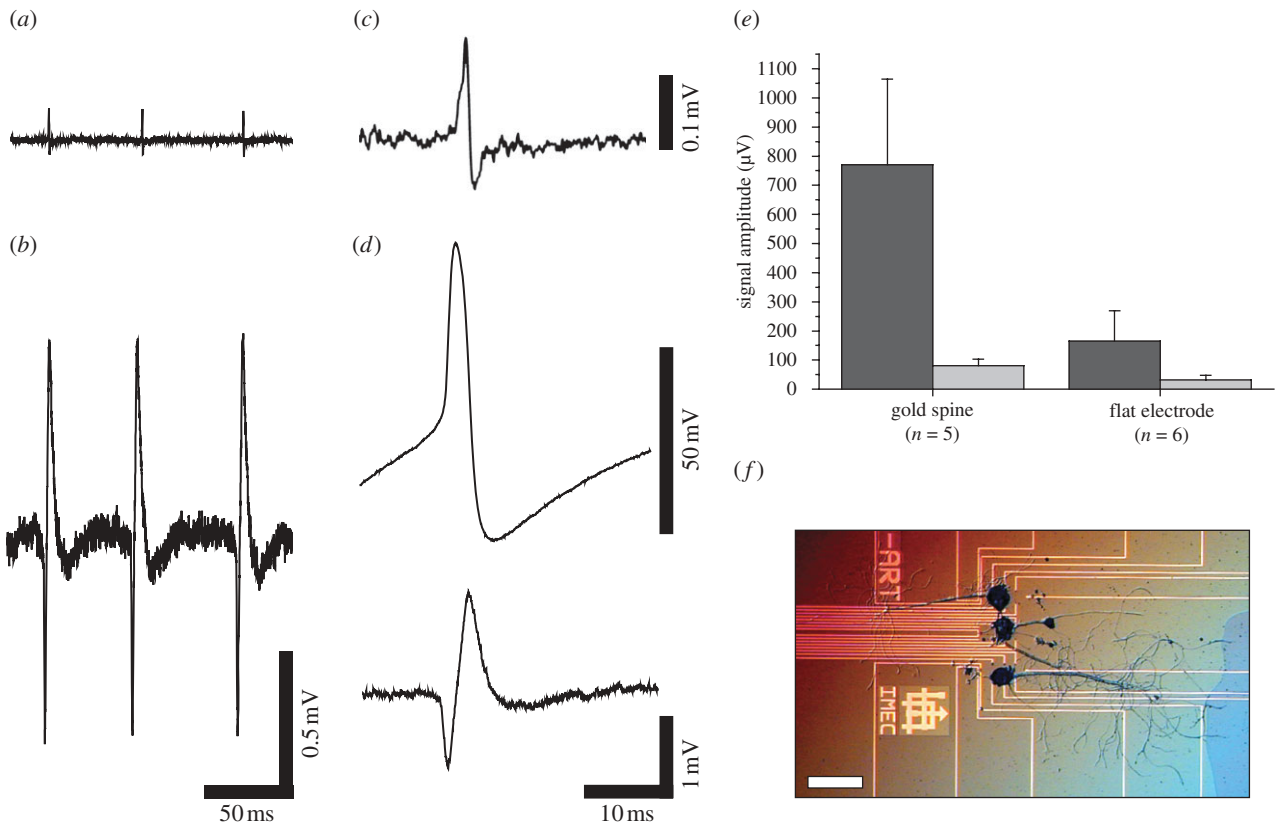


Figure 7. Recording of *Aplysia* LUQ neuron field potentials by commercial flat electrodes and gold-spine electrodes. A train of field potentials recorded by (a) a commercial flat electrode and (b) a four-gold-spine electrode (scale bar in (b) also applies to (a)). (c,d) Single field potentials recorded by a flat electrode and a four-gold-spine electrode, respectively. The upper panel in (d) is the intracellular action potential corresponding to the field potential shown in the bottom panel. (e) Comparison of amplitude (dark grey rectangles, signal amplitude; light grey rectangles, noise amplitude) and signal-to-noise ratio recorded by commercial flat electrodes ($n = 6$) and four-gold-spine electrode sensor ($n = 5$). (f) LUQ neurons from the abdominal ganglion of *A. californica*, cultured on an electrode array of gold spines.

taken in areas where no apparent cleft is visible between the gold spine and the plasma membrane, table 1). For the sake of simplification, we divide the resistance of the cleft into two serially connected resistances: (i) the junction between the neuron and the flat surface of the device and (ii) the junction between the small patches of high adhesion around the gold spine and the spine itself. The latter can be estimated by

$$R = \frac{\rho_j}{2\pi \cdot a_s \cdot d_j} \cdot l, \psi \quad (4.1)$$

where ρ is the specific resistance of the cleft estimated at $100 \Omega \text{ cm}$, a_s the radius of the spine head taken as $0.95 \mu\text{m}$ and l the length of the resistor across which the transductive extracellular current flows and is taken as the circumference of the spine (approx. $4 \mu\text{m}$). Considering the cleft width d_j to be 10 nm , we get from equation (4.1) that the seal resistance in the vicinity of the spine is $R_{\text{seal}} = 67 \text{ M}\Omega$.

According to estimations developed by Weis & Fromherz (1997), the seal resistance of a junction of unknown contact area between a flat surface and the plasma membrane of a neuron can be approximated by

$$R_{\text{seal}} = \frac{\rho_j}{\pi \cdot \Phi \cdot d_j} \cdot \psi \quad (4.2) \leftarrow$$

where Φ is the scaling factor ranging between 4 and 6 (taken here as $\Phi = 5$). Using cleft width $d_j = 55.8 \text{ nm}$ and the same value for ρ_j , we get $R_{\text{seal}} = 2.12 \text{ M}\Omega$. Measurements of the seal resistance formed between entire cultured *Aplysia* neurons and a flat substrate were found to be $1.2 \pm 0.43 \text{ M}\Omega$ (Cohen *et al.* 2008). Thus our estimation suggests that the gold spine neuron junctions improve R_{seal} by more than an order of magnitude.

4.2. The dimensions of the gold-spine-like protrusions limit the current flow across R_{seal}

As mentioned in §1, the electrical coupling between neurons and micro-electronic devices depends on the seal resistance and the current that flows across it. In excitable cells, the current generated by a given patch of plasma membrane is limited by the number of active voltage-dependent ion channels embedded in the plasma membrane. The density of voltage-gated ion channels throughout the plasma membrane is finite. For example, in muscle fibres, the density of the voltage-gated sodium channels was estimated to be 380 channels per μm^2 (Almers & Levinson 1975), whereas in mammalian myelinated nerve fibres, the

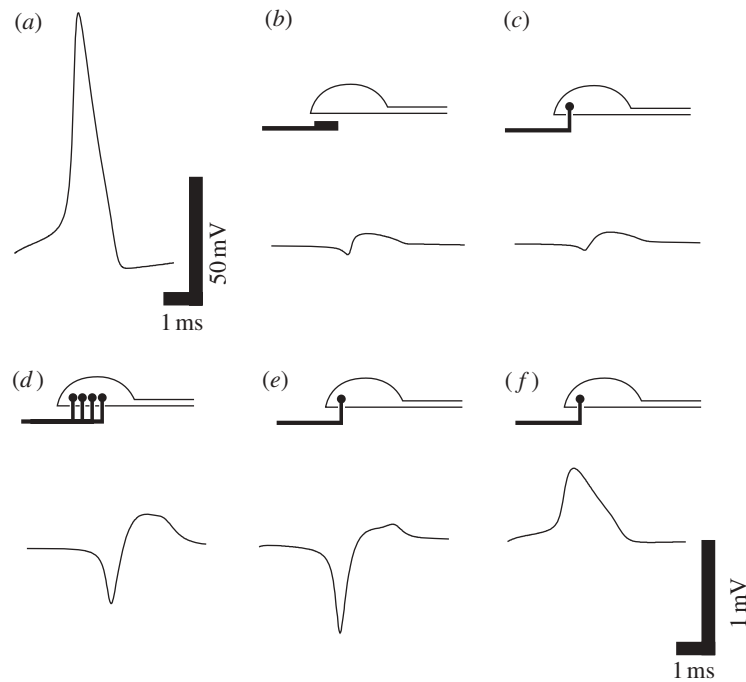


Figure 8. Computer simulations of field potential recordings. A step depolarization pulse (10 nA, 50 ms) generates an action potential and is ‘intracellularly’ recorded at the soma (a). (b) A simulated field potential recorded by a flat electrode with $R_{\text{seal}} = 2.12 \text{ M}\Omega$. (c, d) Simulations of the field potential recorded by an engulfed gold-spine electrode with one and four gold spines at the tip of the electrode, respectively, with $R_{\text{seal}} = 67 \text{ M}\Omega$. (e) A simulated field potential recorded by an engulfed gold-spine electrode with a 50 per cent increase in the density of voltage-gated sodium channels facing the spine. (f) A field potential recorded by an engulfed gold-spine electrode with a 50 per cent increase in the density of passive channels facing the spine (scale bars in b–f are the same).

density of sodium channels can be as high as 12 000 per μm^2 in nodal areas and as low as 25 channels per μm^2 in internodal areas (Ritchie & Rogart 1977). Thus, a disadvantage of electrodes with small surface area is the relatively low current that can be generated by the membrane patch in contact with the electrode or the number of passive ion channels through which current can flow. The estimated gold-spine surface area is approximately $6.88 \mu\text{m}^2$, thus (using the density of sodium channels of muscle fibres) a range of 2500 sodium channels and approximately a similar number of potassium channels ‘face’ the gold spine. A standard large flat electrode with a radius of $10 \mu\text{m}$ has an area of $314 \mu\text{m}^2$ and is thus faced by approximately 120 000 sodium channels. Simulations of field potentials recorded by flat and gold-spine electrodes (figure 8) demonstrate the expected amplitude and shape of the signals acquired by the two types of devices. For the simulation of cultured *Aplysia* neurons, we assumed that the soma expresses 85 per cent of the sodium and potassium densities with respect to the axon and that the axon hillock expresses 117 per cent of the ion channel densities of the axon (Cohen et al. 2006). Under this configuration, a simulated depolarization of the cell body by a step depolarization pulse (10 nA, 50 ms) generates an action potential (figure 8a). The resulting biphasic field potential amplitude recorded at the soma by the flat electrode ($10 \mu\text{m}$ diameter, with $R_{\text{seal}} = 2.12 \text{ M}\Omega$) was approximately $200 \mu\text{V}$ (figure 8b). Simulating a single spine electrode with a circumference of $4 \mu\text{m}$ and a seal resistance of $67 \text{ M}\Omega$

generates simulated field potentials with amplitudes of approximately $180 \mu\text{V}$ (figure 8c). Thus, the estimated value of the seal resistance formed around a single spine–membrane interaction is insufficient to compensate (in terms of peak field potential amplitude) for the relatively small surface area of the electrode and the small number of ion channels facing a single gold spine. It should be noted that the biphasic shapes of the field potentials recorded by the flat electrode and the spine are similar. Simulating the configuration of the four-gold-spine electrodes that increase the contact area between the device and the neurons (while maintaining a seal resistance of $67 \text{ M}\Omega$ per spine) generates a biphasic field potential with an amplitude of approximately $770 \mu\text{V}$ (figure 8d), indicating that the seal resistance formed around the spines along with an overall increase in the number of ion channels facing the four-spines configuration is sufficient to account for the field potential amplitude recorded experimentally.

We next considered two additional mechanisms that could account for the observed increase in the field potential amplitude. These are a local aggregation of voltage-gated sodium channels, or a local increase in voltage-independent channels around the spine’s head. Simulating a field potential recorded by a single gold-spine electrode with a local increase of 50 per cent in the number of voltage-gated sodium channels around the spine resulted in field potential amplitudes of approximately $800 \mu\text{V}$ (figure 8e). It is important to note that this field potential is characterized by a large phase of inward current (negative-phase) in

contrast to the biphasic nature of the experimental results. Simulating field potentials recorded by an engulfed gold-spine electrode with a 50 per cent local increase in passive membrane conductance at the spine head (by aggregation of voltage-independent channels) increases the peak amplitude of the field potential, reaching approximately 650 μV (figure 8f). Under these conditions, however, the field potential is characterized by the large monophasic positive-phase, reminiscent of semi-intracellular recordings (Cohen et al. 2008).

Based on comparison between the field potentials' amplitudes and shapes obtained experimentally and the simulations, it is reasonable to suggest that the increased seal resistance, rather than aggregation of voltage-dependent or -independent channels around the spine head, is the main parameter that underlies the improved electrical coupling. This conclusion is consistent with the ultrastructural analysis that indicated a significant increase in the adhesion of the neurons to the gold-spine substrate.

5. CONCLUSIONS

The combined use of: (i) three-dimensional gold micro-structures that protrude from a flat substrate to imitate 'dendritic spines' by shape and dimensions and (ii) functionalization of the gold-spine structure by a peptide that enhances the naturally occurring phagocytotic activity results in the engulfment of the gold spines by cultured cells. This in turn is associated with improved cell attachment to the three-dimensional substrate, reduction in the dimensions of the cleft formed between the plasma membrane and the gold-spine surface, increase in the estimated value of R_{seal} and improved electrical coupling between neurons and the sensing device.

The use of fundamental cell biological mechanisms that allow living cells to actively respond to external structural and chemical signals, on the one hand, and the presentation of competent three-dimensional micro-structures and surface chemistry, on the other, are expected, as indicated here, to open up new ways to improve bi-directional coupling between cells and electronic devices.

This work was supported by the Golden Brain project (EU no. P6 510574 STREP), the Brain Storm project (EU no. P7 215486 STREP) and a very small part by the FIRST programme no. 1480/07 of the Israel Science Foundation. Parts of the study were carried out at the Charles E. Smith and Prof. Elkes Laboratory for Collaborative Research in Psychobiology. M.E.S. is the Levi DeViali Professor in neurobiology.

REFERENCES

- Almers, W. & Levinson, S. R. 1975 Tetrodotoxin binding to normal depolarized frog muscle and the conductance of a single sodium channel. *J. Physiol.* **247**, 483–509.
- Braun, D. & Fromherz, P. 1997 Fluorescence interference-contrast microscopy of cell adhesion on oxidized silicon. *Appl. Phys. A* **65**, 341–348. (doi:10.1007/s003390050589)
- Braun, D. & Fromherz, P. 2004 Imaging neuronal seal resistance on silicon chip using fluorescent voltage-sensitive dye. *Biophys. J.* **87**, 1351–1359. (doi:10.1529/biophysj.104.039990)
- Brittinger, M. & Fromherz, P. 2005 Field-effect transistor with recombinant potassium channels: fast and slow response by electrical and chemical interactions. *Appl. Phys. A* **81**, 439–447. (doi:10.1007/s00339-005-3272-7)
- Cai, N., Gong, Y., Chian, K. S., Chan, V. & Liao, K. 2008 Adhesion dynamics of porcine esophageal fibroblasts on extracellular matrix protein-functionalized poly(lactic acid). *Biomed. Mater.* **3**, 15014. (doi:10.1088/1748-6041/3/1/015014)
- Cohen, A., Spira, M. E., Yitzchaik, S., Borghs, G., Shwartzglass, O. & Shappir, J. 2004 Depletion type floating gate p-channel MOS transistor for recording action potentials generated by cultured neurons. *Biosens. Bioelectron.* **19**, 1703–1709. (doi:10.1016/j.bios.2004.01.021)
- Cohen, A., Shappir, J., Yitzchaik, S. & Spira, M. E. 2006 Experimental and theoretical analysis of neuron–transistor hybrid electrical coupling: the relationships between the electro-anatomy of cultured *Aplysia* neurons and the recorded field potentials. *Biosens. Bioelectron.* **22**, 656–663. (doi:10.1016/j.bios.2006.02.005)
- Cohen, A., Shappir, J., Yitzchaik, S. & Spira, M. E. 2008 Reversible transition of extracellular field potential recordings to intracellular recordings of action potentials generated by neurons grown on transistors. *Biosens. Bioelectron.* **23**, 811–819. (doi:10.1016/j.bios.2007.08.027)
- Fromherz, P. 2003 Neuroelectronic interfacing: semiconductor chips with ion channels, nerve cells and brain. In *Nanoelectronics and information technology* (ed. R. Waser), pp. 781–810. Weinheim, Germany: Wiley-VCH Verlag.
- Gimsa, U., Iglie, A., Fiedler, S., Zwanzig, M., Kralj-Iglie, V., Jonas, L. & Gimsa, J. 2007 Actin is not required for nanotubular protrusions of primary astrocytes grown on metal nano-lawn. *Mol. Membr. Biol.* **24**, 243–255. (doi:10.1080/09687860601141730)
- Gleixner, R. & Fromherz, P. 2006 The extracellular electrical resistivity in cell adhesion. *Biophys. J.* **90**, 2600–2611. (doi:10.1529/biophysj.105.072587)
- Hines, M. L. & Carnevale, N. T. 1997 The NEURON simulation environment. *Neural Comput.* **9**, 1179–1209. (doi:10.1162/neco.1997.9.6.1179)
- Hodgkin, A. L. & Huxley, A. F. 1952 A quantitative description of membrane current and its application to conduction and excitation in nerve. *J. Physiol. Lond.* **117**, 500–544.
- Huynh, K. K., Kay, J. G., Stow, J. L. & Grinstein, S. 2007 Fusion, fission, and secretion during phagocytosis. *Physiology (Bethesda)* **22**, 366–372. (doi:10.1152/physiol.00028.2007)
- Huys, R. et al. 2008 Novel concepts for improved communication between nerve cells and silicon electronic devices. *Solid State Electron.* **52**, 533–539. (doi:10.1016/j.sse.2007.10.025)
- Iwanaga, Y., Braun, D. & Fromherz, P. 2001 No correlation of focal contacts and close adhesion by comparing GFP-vinculin and fluorescence interference of Dil. *Eur. Biophys. J.* **30**, 17–26. (doi:10.1007/s002490000119)
- Jenkner, M. & Fromherz, P. 1997 Bistability of membrane conductance in cell adhesion observed in a neuron-transistor. *Phys. Rev. Lett.* **79**, 4705–4708. (doi:10.1103/PhysRevLett.79.4705)
- Lambacher, A. & Fromherz, P. 1996 Fluorescence interference contrast microscopy on oxidized silicon using a monomolecular dye layer. *Appl. Phys. A* **63**, 207–216. (doi:10.1007/BF01567871)
- Lim, J. Y. & Donahue, H. J. 2007 Cell sensing and response to micro- and nanostructured surfaces produced by chemical and topographic patterning. *Tissue Eng.* **13**, 1879–1891. (doi:10.1089/ten.2006.0154)

- Matus, A. 2005 Growth of dendritic spines: a continuing story. *Curr. Opin. Neurobiol.* **15**, 67–72. (doi:10.1016/j.conb.2005.01.015)
- McMahon, H. T. & Gallop, J. L. 2005 Membrane curvature and mechanisms of dynamic cell membrane remodelling. *Nature* **438**, 590–596. (doi:10.1038/nature04396)
- Oren, R. *et al.* 2004 Electrically conductive 2D-PAN-containing surfaces as a culturing substrate for neurons. *J. Biomater. Sci. Polym. Ed.* **15**, 1355–1374. (doi:10.1163/1568562042368077)
- Ritchie, J. M. & Rogart, R. B. 1977 Density of sodium channels in mammalian myelinated nerve fibers and nature of the axonal membrane under the myelin sheath. *Proc. Natl Acad. Sci. USA* **74**, 211–215. (doi:10.1073/pnas.74.1.211)
- Roelandse, M., Welman, A., Wagner, U., Hagmann, J. & Matus, A. 2003 Focal motility determines the geometry of dendritic spines. *Neuroscience* **121**, 39–49. (doi:10.1016/S0306-4522(03)00405-6)
- Schacher, S. & Proshansky, E. 1983 Neurite regeneration by Aplysia neurons in dissociated cell culture: modulation by Aplysia hemolymph and the presence of the initial axonal segment. *J. Neurosci.* **3**, 2403–2413.
- Sniadecki, N. J., Desai, R. A., Ruiz, S. A. & Chen, C. S. 2006 Nanotechnology for cell–substrate interactions. *Ann. Biomed. Eng.* **34**, 59–74. (doi:10.1007/s10439-005-9006-3)
- Spatz, J. P. & Geiger, B. 2007 Molecular engineering of cellular environments: cell adhesion to nano-digital surfaces. *Methods Cell Biol.* **83**, 89–111. (doi:10.1016/S0091-679X(07)83005-6)
- Spira, M. E., Dormann, A., Ashery, U., Gabso, M., Gitler, D., Benbassat, D., Oren, R. & Ziv, N. E. 1996 Use of *Aplysia* neurons for the study of cellular alterations and the resealing of transected axons *in vitro*. *J. Neurosci. Methods* **69**, 91–102. (doi:10.1016/S0165-0270(96)00024-6)
- Spira, M. E., Oren, R., Dormann, A. & Gitler, D. 2003 Critical calpain-dependent ultrastructural alterations underlie the transformation of an axonal segment into a growth cone after axotomy of cultured *Aplysia* neurons. *J. Comp. Neurol.* **457**, 293–312. (doi:10.1002/cne.10569)
- Straub, B., Meyer, E. & Fromherz, P. 2001 Recombinant maxi-K channels on transistor, a prototype of iono-electronic interfacing. *Nat. Biotechnol.* **19**, 121–124. (doi:10.1038/84369)
- Stuart, L. M. & Ezekowitz, R. A. 2005 Phagocytosis: elegant complexity. *Immunity* **5**, 539–550. (doi:10.1016/j.immuni.2005.05.002)
- Studer, D., Humbel, B. M. & Chiquet, M. 2008 Electron microscopy of high pressure frozen samples: bridging the gap between cellular ultrastructure and atomic resolution. *Histochem. Cell Biol.* **130**, 877–889. (doi:10.1007/s00418-008-0500-1)
- Toublan, F. J., Boppart, S. & Suslick, K. S. 2006 Tumor targeting by surface-modified protein microspheres. *J. Am. Chem. Soc.* **128**, 3472–3473. (doi:10.1021/ja0544455)
- Wang, L. & Sigworth, F. J. 2006 Cryo-EM and single particles. *Physiology (Bethesda)* **21**, 13–18. (doi:10.1152/physiol.00045.2005)
- Weis, R. & Fromherz, P. 1997 Frequency dependent signal transfer in neuron transistors. *Phys. Rev. E* **55**, 877–889. (doi:10.1103/PhysRevE.55.877)
- Wrobel, G., Höller, M., Ingebrandt, S., Dieluweit, S., Sommerhage, F., Bochem, H. P. & Offenhäusser, A. 2008 Transmission electron microscopy study of the cell–sensor interface. *J. R. Soc. Interface* **5**, 213–222. (doi:10.1098/rsif.2007.1094)
- Ziv, N. E. & Spira, M. E. 1998 Induction of growth cone formation by transient and localized increases of intracellular proteolytic activity. *J. Cell Biol.* **140**, 223–232. (doi:10.1083/jcb.140.1.223)